Repeated Profiling of Microstructure Lenses with a Midwater Float

GORDON O. WILLIAMS

Institute of Geophysics and Planetary Physics, Scripps Institution of Oceanography, University of California, La Jolla 92093

(Manuscript received 11 July 1975, in revised form 16 December 1975)

ABSTRACT

A freely drifting, midwater float equipped with a buoyancy controller has been developed and used to obtain 20 m profiles of temperature gradient (~0.02 m resolution) and temperature (~0.5 m resolution) at ~6 min intervals. Thermal structure and internal wave motions from a 20 h record obtained at 550 m depth and 500 km offshore from Southern California are analyzed. Intense microstructure activity is episodic and concentrated into microstructure "lenses." Two of three lenses of increased microstructure activity found were associated with intrusions of ~5 m vertical and ~100 m horizontal scale. A third, much smaller and weaker lens was associated with a temperature step. A hint that microstructure intensity was modulated by low-frequency internal wave shear is also found.

1. Introduction

A freely drifting, "Yo-Yo-ing" midwater float has been developed and used to make repeated thermal microstructure and temperature profiles of a ~20 m segment of the water column at ~6 min intervals. A 20 h record obtained at a center depth of 550 m on 8 June 1973 at 30°40'N, 121°28'W, about 500 km southwest of San Diego, Calif., is discussed (Fig. 1). These measurements augment previous oceanic microstructure work using free-fall instruments in which dissipation rates (Osborn and Cox, 1972) and the vertical wavenumber spectrum of temperature fluctuations (Gregg *et al.*, 1973) have been studied.

2. Experimental procedure

The float (Fig. 2) is a carefully ballasted Deep Sea Tides Capsule (Snodgrass, 1968) equipped with a new data-logger, a buoyancy control cannister (Fig. 3), and control logic to make repeated profiles of a vertical segment of the thermal structure. The ballasting and buoyancy cannister development were done jointly with James Cairns who has conducted somewhat related experiments (Cairns, 1975).

The sensor array, suspended beneath the float, is equipped with two thermal microstructure sensors and three quartz thermometers. The sensing element of each of the two microstructure temperature gradient sensors is a high-speed thermistor enclosed in a 0.5 mm diameter glass rod. These sensors are essentially similar to those described by Cox *et al.* (1969). The temperature and pressure sensors are of the quartz crystal type and previously have been described by Caldwell *et al.* (1969) and Irish and Snodgrass (1972) respectively.

The microstructure sensors are sampled at 0.1 s intervals; the remaining sensors are sampled at 4 s intervals. The sampling rates, sensor response times, and the profiling velocity yield vertical spatial resolutions of ~0.02 m and ~0.5 m for the microstructure sensors and quartz thermometers respectively. The pressure sensor data least count is 27.5 mm. Data are stored in the capsule in standard computer compatible format on a 732 m reel of 12.7 mm computer tape.

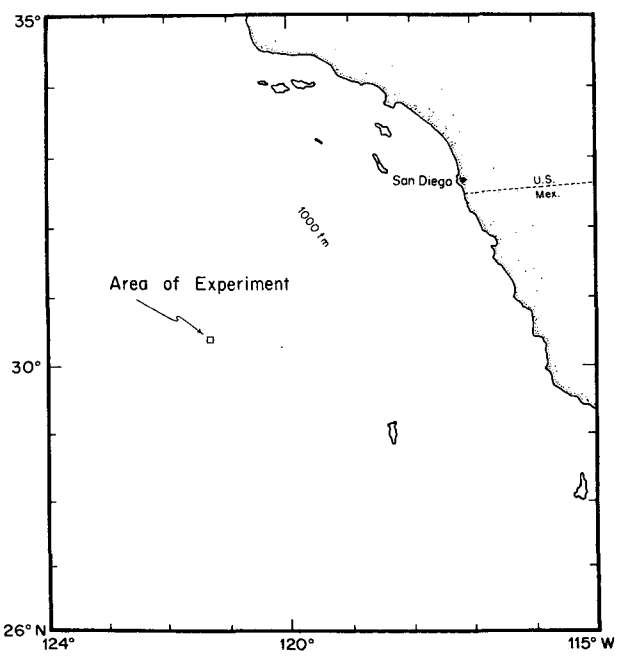

FIG. 1. Map of the experimental area.

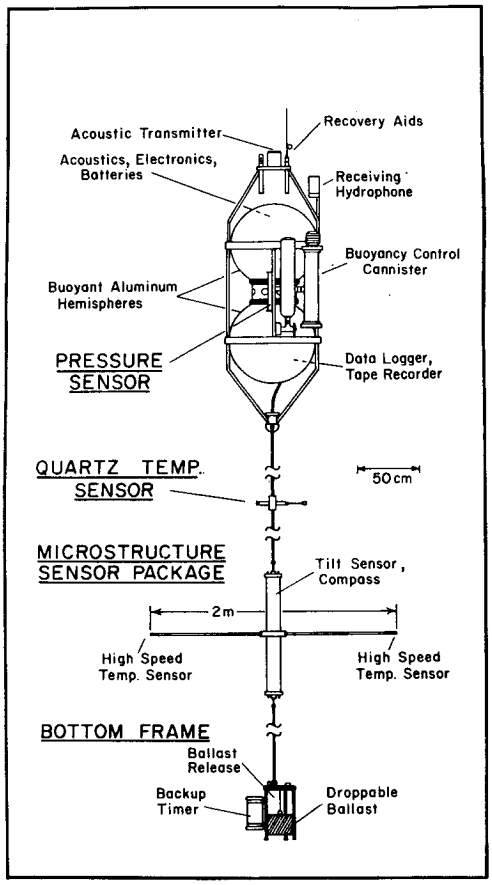

FIG. 2. Yo-Yo-ing midwater float. For vertical scale see Fig. 4.

The sensor and control logic arrangement used result in a central 20 m region profiled by the microstructure sensors every ~6.4 min on average (Fig. 4). This region is also profiled by a quartz thermometer every ~3 min on average. Above and below the central region are 10 m regions profiled by a quartz thermometer every 6.4 min on average.

The profiling is accomplished as follows:

1) After launch the capsule, with the buoyancy cannister set at the center of its range, settles to its equilibrium depth.

2) Upon acoustic command from the surface, the temperature seen at that moment by the center quartz thermometer (Fig. 4, Temp. 2) is stored in the capsule's memory. This temperature becomes the reference isotherm for the depth control logic.

3) A second acoustic command enables the control logic which causes the capsule to first rise for 6.4 min and then to sink until a temperature lower than that of the reference isotherm has been found for a total of 64 s.

The capsule is then made to rise for 6.4 min, etc. This cycle continues as long as the control logic is enabled. Additional details are found in Williams (1975).

3. Spatial and temporal ambiguity

In general the sensors are slowly towed laterally relative to the water at their depth because of the presence of vertical shear. The data, therefore, contain a mixture of temporal and spatial effects. We consider now the nature of the mixture.

The horizontal towing velocity of a sensor depends on its vertical distance from the center of horizontal drag of the system (~20 m above the central sensor) and on the magnitude of the shear. The horizontal drift velocity of the central sensor is estimated to be on the order of 0.01 m s^{-1}. This estimate is based upon both direct measurements made with an electromagnetic current meter (Olson, 1972) on a later cruise and on the following calculation using the GM72 and GM75 internal wave spectra (Garrett and Munk, 1972a, 1975). The mean square difference in the horizontal water velocity over a depth interval z_0 is given by

$$\langle \Delta u^2 \rangle = \langle [u(z+z_0) - u(z)]^2 \rangle = 2[R(0) - R(z_0)],$$

where

$$R(z) = \int_0^\infty F_u(\beta) e^{i2\pi\beta z} d\beta$$

is the autocovariance of $u(z)$ and $F_u(\beta)$ the spectrum of

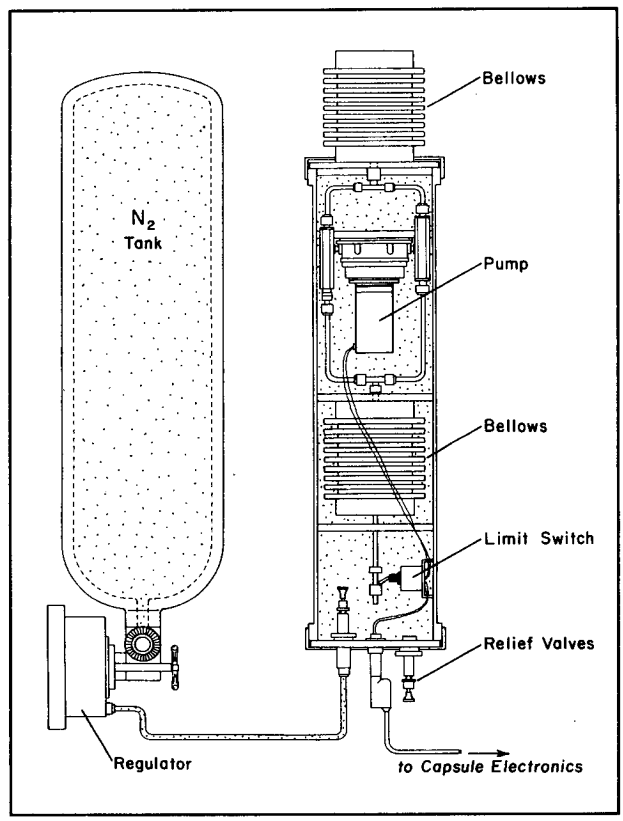

FIG. 3. Buoyancy cannister used to vary the volume and density of the capsule system.

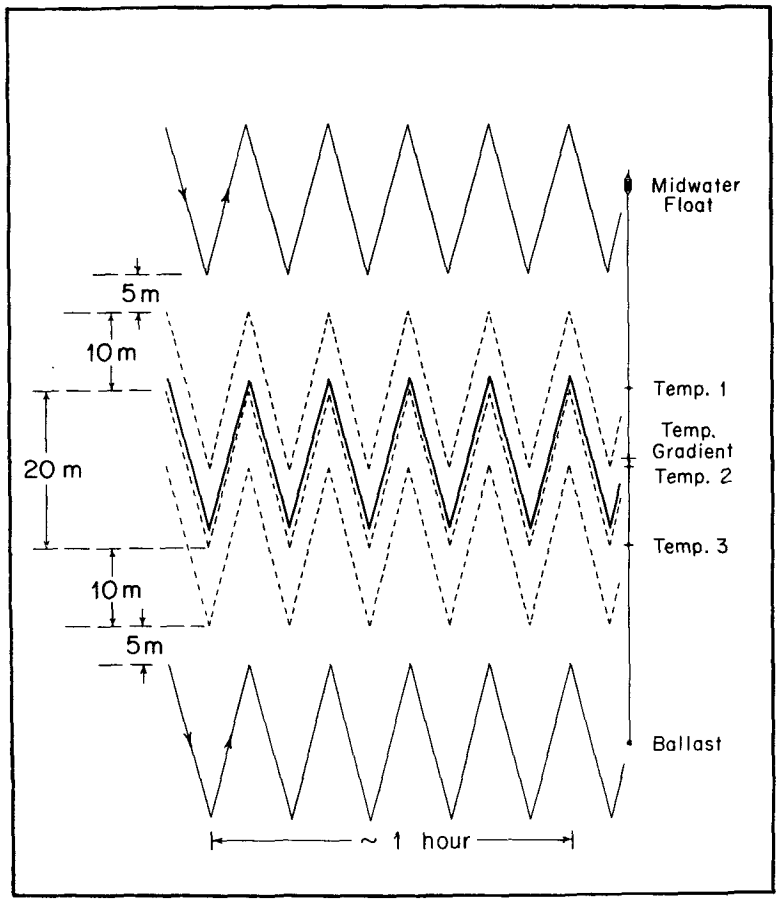

FIG. 4. Depth coverage of the temperature and temperature gradient sensors (schematic).

horizontal velocity. Carrying out the indicated operations for $z_0 = 20$ m yields

$$\langle \Delta u^2 \rangle^{\frac{1}{2}} = 0.02,\ 0.016 \text{ m s}^{-1}$$

for GM72 and GM75, respectively.

The actual distance made good by the sensors is a function of both the magnitude of the drift velocity and the frequency and size of changes in direction of the drift. The sharp cusp near the inertial frequency in the internal wave spectrum suggests that the radius of curvature of the capsule motion is large. W. Munk (personal communication) finds the motion to be quasi-circular with radius O(1 km).

The mean time rate of change of the thermal structure has been estimated from the microstructure data using the model of Osborn and Cox (1972). A vertical temperature variation, $\cos\beta z$, decays to e^{-1} of its amplitude in a time $k_z^{-1}\beta^{-2}$. Calculated e^{-1} decay times (Table 1) indicate that temperature features with vertical wavelengths $\gtrsim 1$ m are little changed by mixing for periods of several hours. No rapid changes in such features are observed as would be caused by stirring (e.g., overturns) as distinguished from mixing. Spatial and temporal ambiguity in the present data are summarized as follows: several hours of the data can be regarded as an essentially straight line cut through the "frozen" gross ($\gtrsim 1$ m wavelength) thermal structure.

4. Thermal structure

a. *A warm water intrusion*

The microstructure temperature gradient data are discussed in a context established by data from the three quartz thermometers; three overlapping segments of the 20 h record are examined. To emphasize the thermal structure it is convenient to suppress the internal wave field (Fig. 5). The conspicuous tempera-

TABLE 1. Calculated e^{-1} decay times for (top) molecular diffusivity, (middle) the present data, and (bottom) San Diego Trough data (Gregg *et al.*, 1973).

k_z (m^2 s^{-1})	$\lambda = 2\pi/\beta$ 0.05 m	0.1 m	0.5 m	1 m	5 m
1.4×10^{-7}	8 min	30 min	13 h	50 h	52 days
1.3×10^{-6}	5 s	19 s	8 min	32 min	14 h
3.7×10^{-6}	2 s	7 s	3 min	11 min	5 h

ture inversion in Fig. 5 prior to 0345 is shown in greater detail in Fig. 6 (top). This temperature inversion may, at first glance, suggest a density inversion and some kind of a breaking wave. However, the "breaking time" should be on the order of the bulk Väisälä period (30 min), whereas the duration is 2 h.

The inversion may more plausibly be interpreted as a snapshot of part of a warm water intrusion rather than an unusually large density inversion (Gregg and Cox, 1972; Pingree, 1972). Most likely the water of the temperature anomally, slightly overcompensated by salinity, intrudes downward from left to right into water of slightly lower density. Assuming 0.01 m s^{-1} lateral sensor drift, the horizontal extent of the inversion in the direction of sensor drift is ~100 m with aspect ratio ~20:1. The downward slope of the inversion relative to the upper isotherm in Fig. 5 is ~$\frac{1}{4}$ the apparent slope.

The associated microstructure profiles (Fig. 6, middle) show a conspicuous microstructure "lens" (the most extensive in all the data) roughly delineated by the 5.420°C isotherm and coterminous with the warm water intrusion. The left half of the lens is characterized by a very sharp lower boundary. The presence of a sharp *lateral* boundary is indicated by the sudden extinction of the high microstructure activity at 0345.

The active region consists of two adjoining patches of high microstructure activity centered on the maximum of the temperature inversion (Fig. 7). This central "valley" of low mean square gradient separating two peaks in the mean square gradient is present (Fig. 8) wherever the identity of the intrusion core is well defined (see Fig. 6). The significance of the fact that the peak at greater depth is generally larger and less variable in amplitude than the upper peak is not known.

Overall, the two microstructure sensors see comparable structure. However, between the two sensors there is a marked difference in details in the high mean square gradient lens (Fig. 8) indicating that the component features have a horizontal extent small compared to the 2 m sensor separation, i.e., the lens appears to be horizontally patchy as well as being itself a vertical patch of increased activity. Horizontal coherence is discussed in a separate report (Williams, 1976).

The lower boundary of the intrusion (Fig. 6, bottom) is consistently sharp; the boundary of the upper part, by contrast, is less sharp and considerably more variable. Again apparent in this display is the blunt front end of

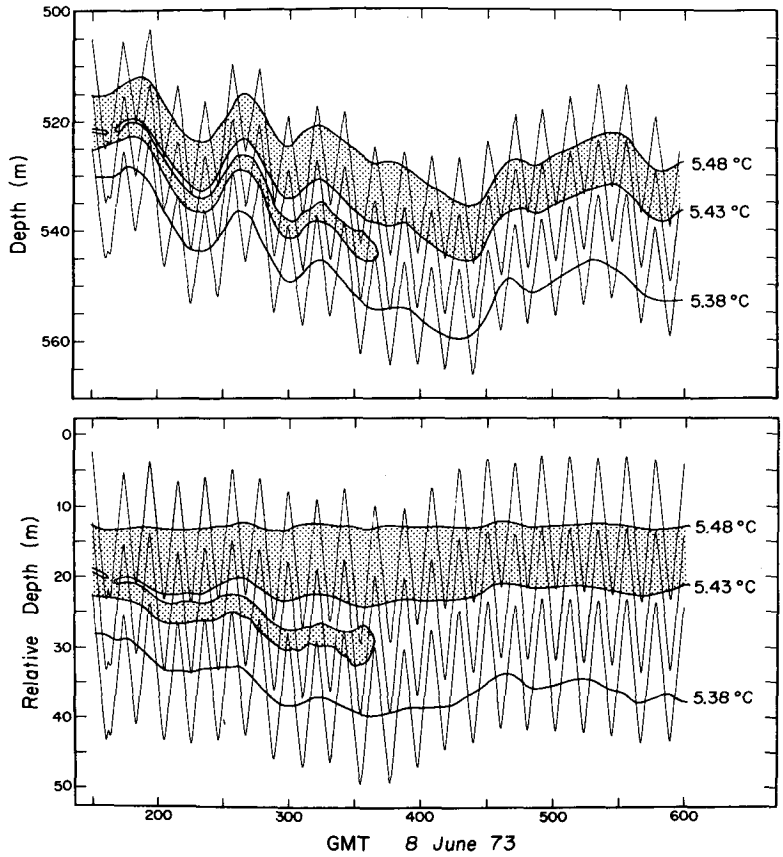

FIG. 5. Depth-time histories of stated isotherms from quartz thermometers. The thermometer tracks are also shown. In the lower display the effect of internal waves has been largely suppressed by referring depths to a 5.490°C reference isotherm.

the temperature inversion. The disappearance of the temperature inversion between profiles indicates a horizontal gradient equal to or larger than the mean *vertical* temperature gradient at that depth.

The bimodal microstructure pattern in the lens described could be associated with either double-diffusive convection or with shear instabilities. A double-diffusive explanation of the bimodal pattern relies principally on the observation that the temperature inversion is gravitationally stable. As noted by Turner (1973, p. 272), intrusions having small density differences with the surrounding water represent particularly favorable circumstances for double-diffusive convection. Thus, one may imagine the diffusive and fingering regimes in operation on the upper and lower half of the intrusion, respectively. How these mechanisms might relate to variations in the observed mean square gradients (Fig. 8) is unknown. However, the internal wave data (discussed below) indicate high vertical shear for this data segment, a situation less favorable to double-diffusive convection (Linden, 1973).

A bimodal microstructure pattern would also be generated if the intrusive velocity led to shear instabilities above and below the core of the intrusion. Two small, sharp temperature inversions in Profile 1 (labeled I and II, Fig. 6) are suggestive of small shear instabilities of <0.5 m scale as discussed by Woods and

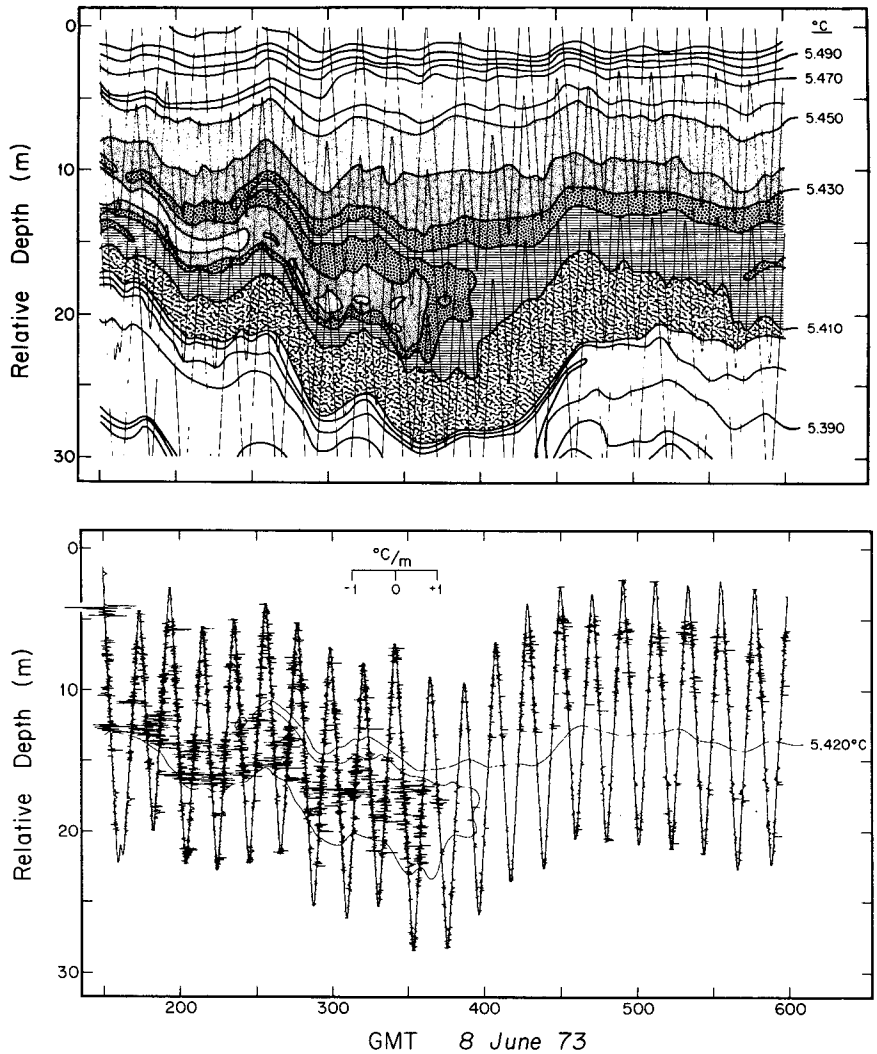

FIG. 6. (Top) Suppressed-wave isotherm contours of Profiles 1–42 at 0.01°C intervals. Sensor depth-time tracks indicate sampling rate. Temperature intervals between isotherms are variously shaded for ease of identification. For comparison, the 5.420°C isotherm is reproduced in the middle and bottom displays. (Middle) The corresponding microstructure temperature gradient profiles. The zero gradient line is along the inclined depth-time track of the microstructure sensor. (Bottom) Integrated microstructure temperature gradient profile. Successive profiles are offset arbitrary distances; times are approximate.

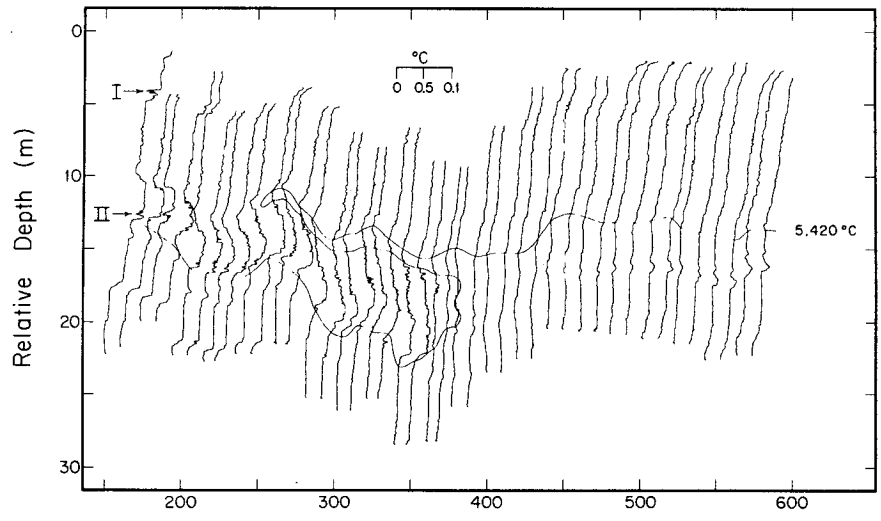

FIG. 6. *Continued.*

Wiley (1972); similar sharp inversions are found in other profiles.

b. A cold water intrusion

The main feature of the second data segment (Fig. 9) is also an intrusion; here there is no hint of the blunt end found in Fig. 6 and the cold water part has a greater vertical extent than the warm water part. An intrusive velocity component perpendicular to the cut through the thermal structure shown is inferred to account for the discontinuous "blobs" of water warmer than 5.470°C from 0930 to 1115.

The depth intervals between isotherms on the far left and far right hand sides of Fig. 9 (top) show marked changes. For example, the depth-interval between the 5.420 and 5.460°C isotherms decreases from 8 to 2 m. Such changes require one or a combination of the following events: (i) fluid convergence or divergence,

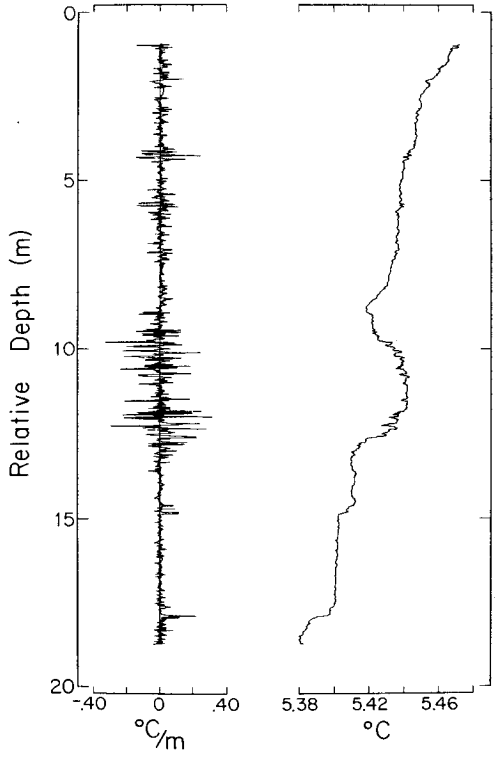

FIG. 7. A single microstructure profile recorded at ~0220: (left) temperature gradient profile; (right) integrated temperature gradient profile.

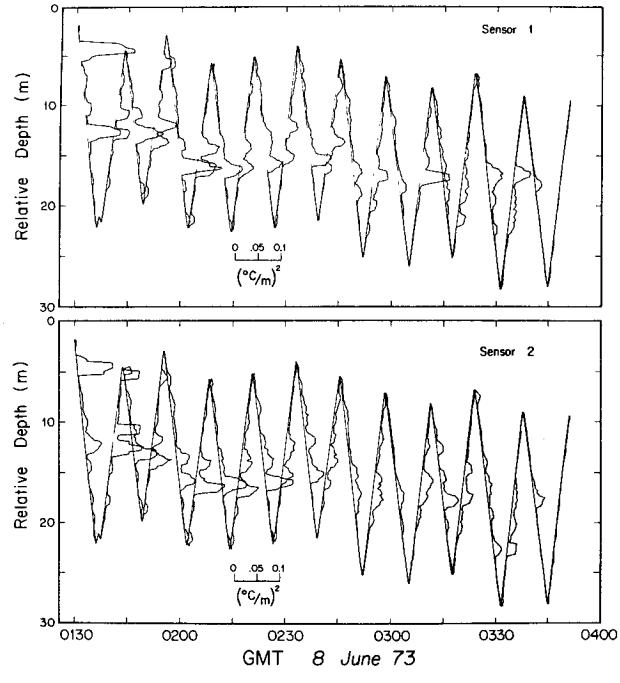

FIG. 8. The mean square temperature gradient (Profiles 1–22) for the two microstructure sensors separated horizontally by 2 m (Fig. 2). The mean square gradient, taken over 1 m intervals, is plotted as a displacement to the right of the sensor depth-time track.

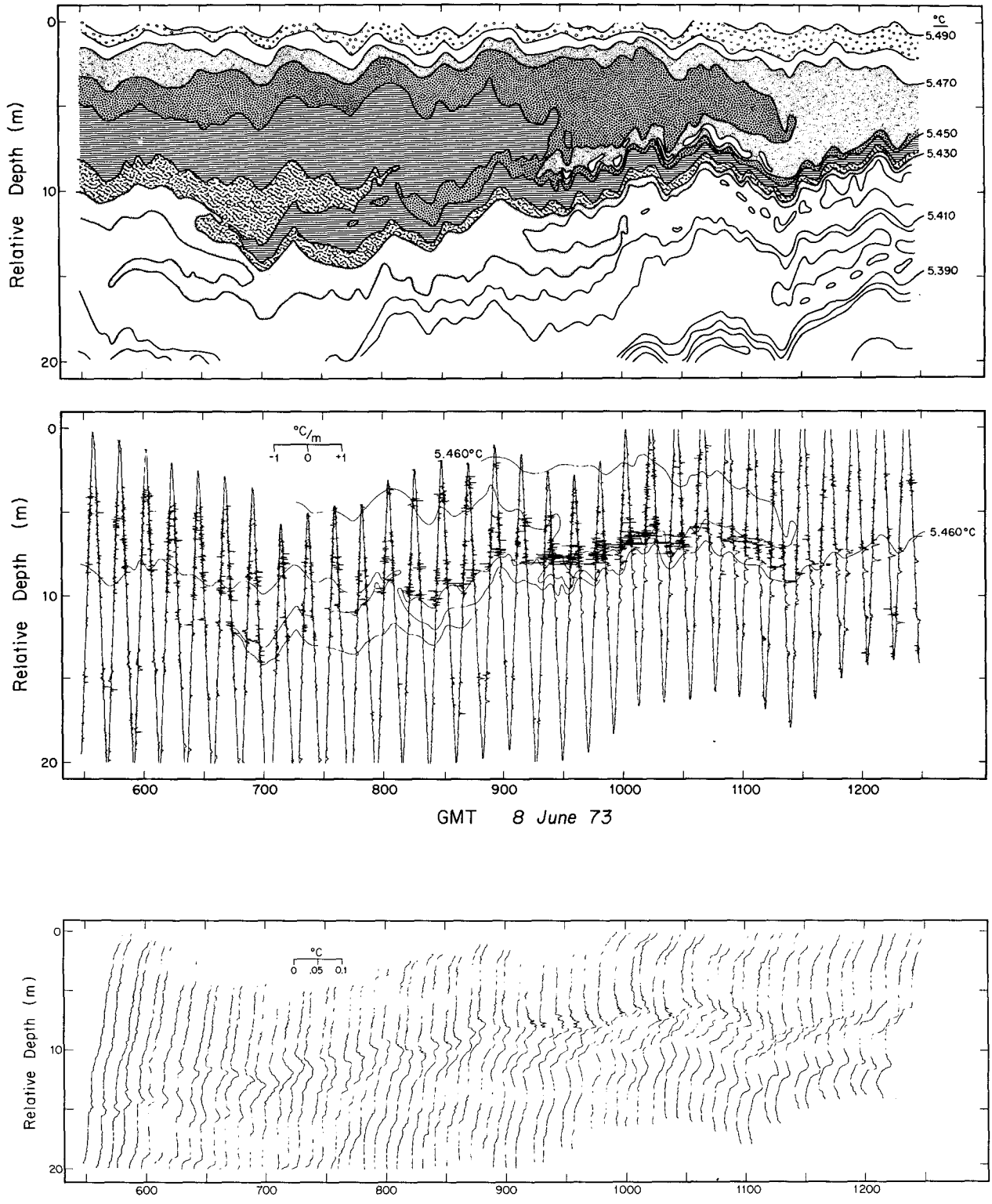

FIG. 9. (Top) Suppressed-wave isotherm contours of Profiles 38–101. (Middle) Corresponding microstructure profiles. Parts of three isotherms with 0.01°C separation have been reproduced from above. (Bottom) Integrated microstructure temperature gradient profiles. Successive profiles are offset arbitrary distances; times are approximate.

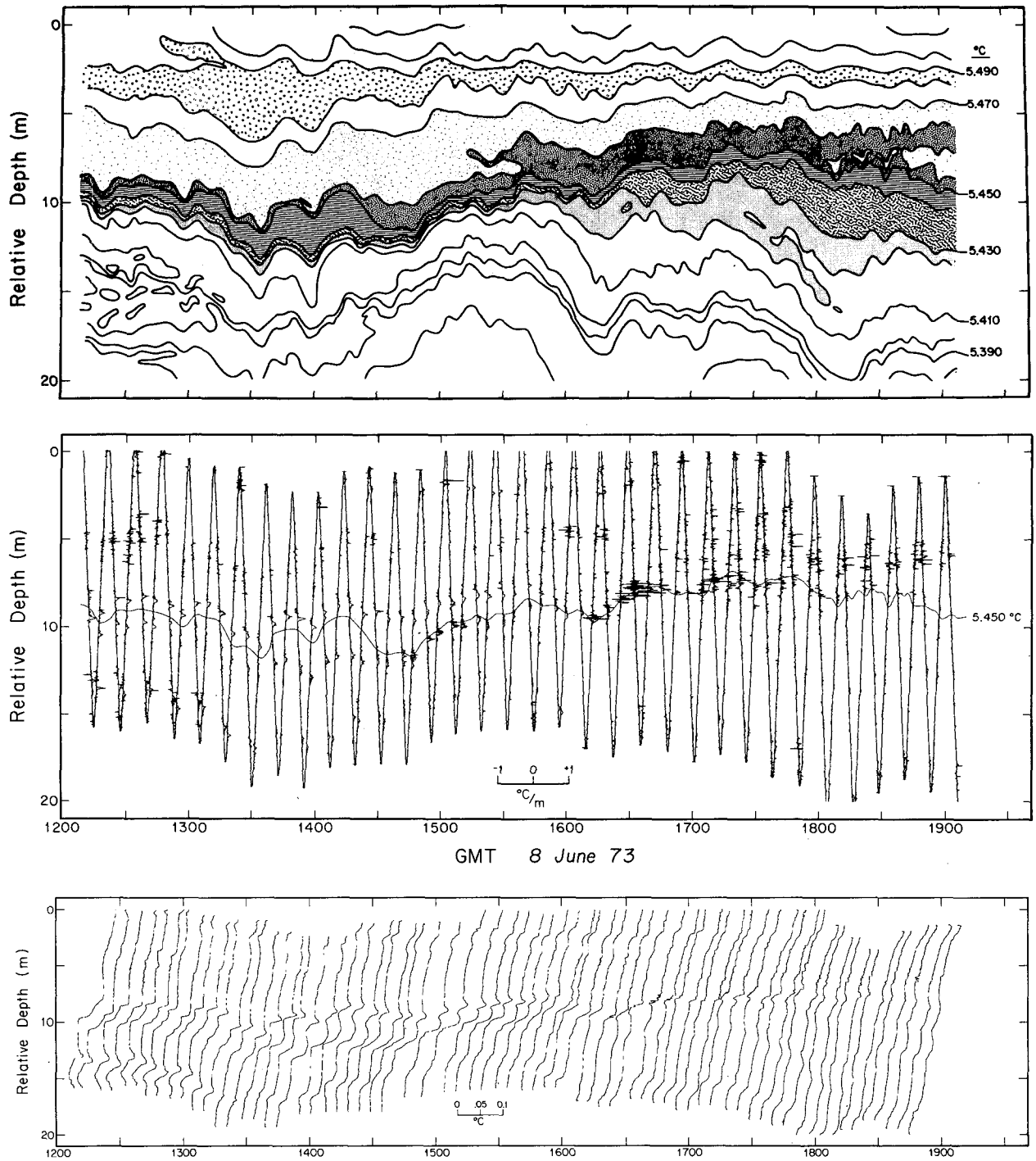

FIG. 10. As in Fig. 9 except for Profiles 99–165. The 5.450°C isotherm (middle) is reproduced from above.

(ii) vertical mixing, or (iii) sensor movement into a water mass with a different T-S relation. Convergence and divergence would require unreasonably high values of vertical strain and very short vertical wavelengths. Intense local mixing is not found at the time of observation. Most probably the sensors have moved out of one water mass and into another. Fig. 9, then, is a snapshot of the boundary between water masses. The feature gives the appearance of being the result of vertical shearing at $\sim$ 8 m relative depth.

The microstructure associated with this intrusion (Fig. 9, middle) is much weaker than for the case previously shown (Fig. 6). A small microstructure lens occurring under conditions consistent with the diffusive

regime from 0915 to 1040 shows no indication of bimodality. Just beneath the lens is a short section of ~1 m "stair steps" (Fig. 9, bottom) suggestive of the fingering regime. These steps, particularly after 1100, appear to bridge the temperature difference between water masses located above and below the steps. The same interpretation is suggested by a noticeable difference in the overall microstructure activity in the top and bottom halves of Fig. 9 (middle). Curiously, details of the bottom, shaded isotherm interval in Fig. 9 (bottom) are not inconsistent with a reversal of the sensor lateral drift direction at ~0800 GMT and of a retracing of the same structure, whereas the upper part of the figure gives no such indication of a drift reversal.

c. *A shear instability*

A third data segment (Fig. 10) is devoid of large inversions or other prominent features. Nevertheless, the corresponding microstructure plot contains a lens centered at 1630. The short section of stair steps pointed out in Fig. 9 (bottom) slowly changes character in Fig. 10 (bottom) thinning down to a single step at 1550. The sharpness of this temperature step increases in time until the microstructure lens appears at 1615. Details of the profiles through the lens are consistent with shear instabilities as described by Woods and Wiley (1972). A step of equal or greater sharpness is observed at an earlier time (1230 to 1400) but without the appearance of a microstructure lens. Time variations in internal wave shear, as discussed in a following section, offer a plausible explanation for the appearance of a microstructure lens in one case but not in the other.

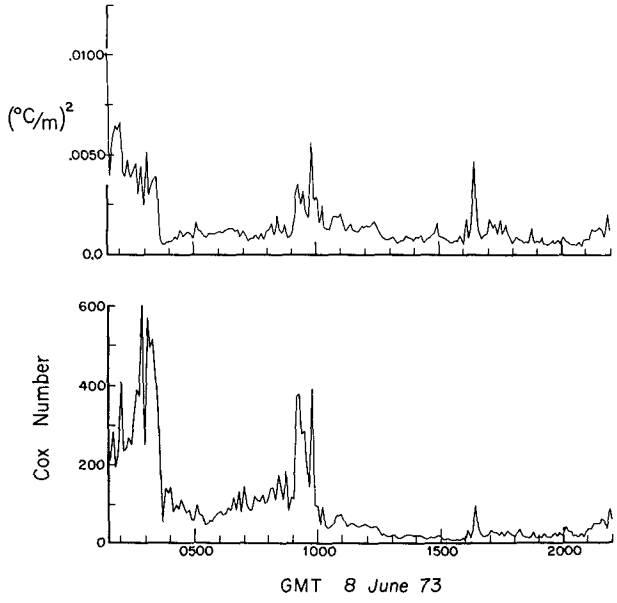

FIG. 11. Microstructure activity averaged for each profile: (top) temperature gradient variance computed from sensor 1 data, (bottom) the same data normalized by the mean temperature gradient of each profile.

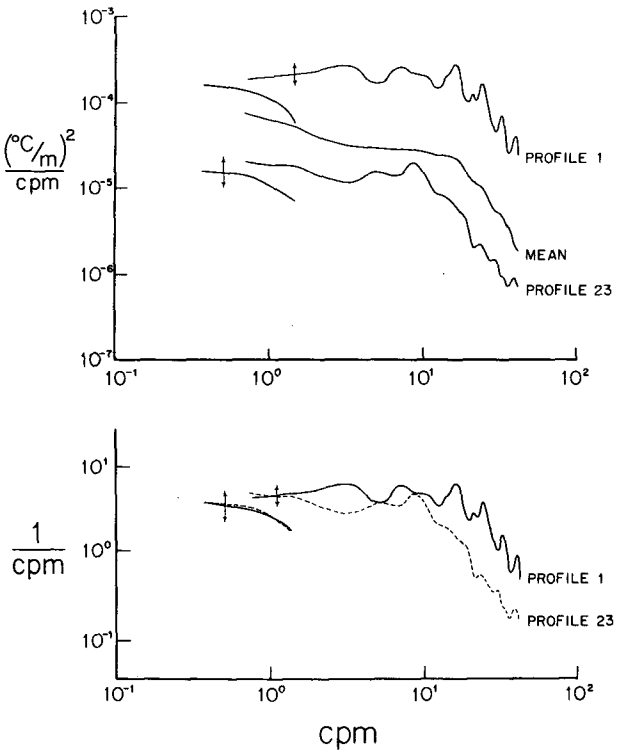

FIG. 12. (Top) Temperature gradient spectra computed from microstructure sensor 1 data for Profiles 1, 23, and the mean spectrum from 193 profiles. Spectra from first-differenced quartz thermometer data are shown as short lines (Profiles 1 and 23). (Bottom) Spectra of Profiles 1 and 23 normalized by the mean gradient squared for each profile, respectively.

5. Normalized microstructure

Three peaks in the mean square gradient (Fig. 11) correspond to the three microstructure lenses (Figs. 6, 9 and 10). The third peak is much less pronounced when the temperature gradient variance is divided by the mean gradient squared (the Cox number). This ratio ranges from 10 to 600 with the mean, 93, falling between the value of 300 obtained for the San Diego Trough and that of 2 obtained for the North Pacific Sub-Tropical Gyre by Gregg *et al.* (1973). Since the highest wavenumber contributions to the variance are not fully resolved in any of these experiments, the Cox numbers are only approximately comparable.

Spectra of temperature gradients vary by 10–15 dB between the "busiest" and the "quietest" profiles (Fig. 12, top). The high-frequency end of the spectrum is estimated to be ~6 dB down because of effects of decreasing thermistor response (Williams, 1975). The spectral "gap" found by Gregg *et al.* (1973) with their free-fall instrument is found only in the quietest profiles, e.g., a slight minimum at 3 cycles per meter (cpm) in Profile 23. The normalized spectral levels (Fig. 12, bottom) show a fair agreement for wavenumbers up to ~10 cpm. Above ~10 cpm the busy and quiet profile spectra diverge slowly leading to a 5 dB difference at

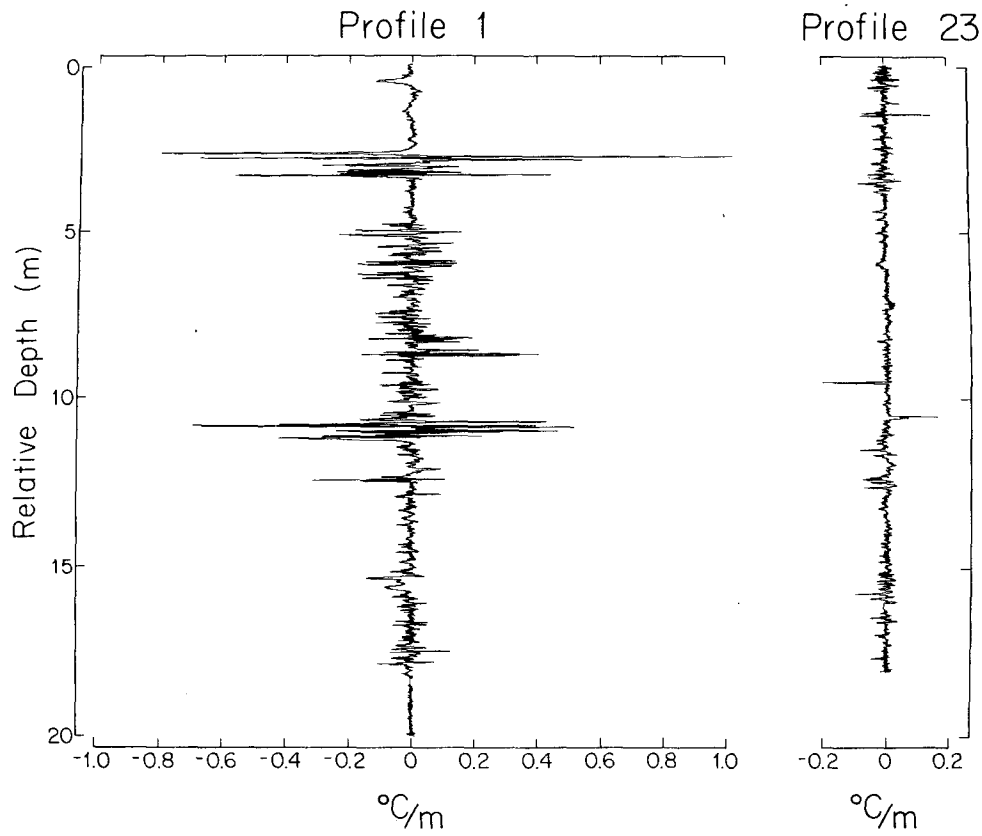

FIG. 13. The "busiest" and "quietest" profiles of microstructure temperature gradient in the 20 h of data. Profile 1 includes the largest peak in temperature gradient.

the high-wavenumber end. The low-wavenumber spectrum is not an overly good predictor of high-wavenumber spectral levels as the shape of the spectra is not constant. For reference, Profiles 1 and 23 are reproduced in Fig. 13.

6. Internal waves

We use the available data to look at time variations of internal wave shear taking a model of the internal wave field with vertical standing and horizontal traveling waves. The component velocities and vertical displacements for internal wave modes propagating horizontally in direction ϕ are

$$\begin{bmatrix} u_1 \\ u_2 \\ \zeta \end{bmatrix} = \mathrm{Re} \begin{bmatrix} iU_L(y)\cos\phi - U_T(y)\sin\phi \\ iU_L(y)\sin\phi + U_T(y)\cos\phi \\ iZ(y) \end{bmatrix} \times \exp[i(\alpha_1 x_1 + \alpha_2 x_2 - \omega t)],$$

where U_L, U_T, Z are real functions of y (Garrett and Munk, 1972a). The vertical strain is

$$\zeta_y = \zeta Z'(y)/Z(y)$$

and the total vertical shear is

$$(u_{1_y}^2 + u_{2_y}^2)^{\frac{1}{2}} = \mathrm{Re}[i(U_L'^2 - U_T'^2)^{\frac{1}{2}}] \exp[i(\alpha_1 x_1 + \alpha_2 x_2 - \omega t)]$$

where $U_L'^2 \geqslant U_T'^2$. Thus, in this model, vertical displacements, vertical strain and vertical shear *magnitudes* are in phase, a relation which permits variations in vertical shear magnitude to be inferred from displacement or temperature gradient data. The internal wave shear spectrum is heavily weighted toward the lower frequencies; in addition, temperature gradient variations have less high-frequency content than displacements (Garrett and Munk, 1972a). Therefore, temperature gradient variations arising from vertical straining are a better indicator of the important, low-frequency vertical shear than vertical displacements of isotherms.

The observed low-frequency vertical displacements and temperature gradient variations (Fig. 14) are roughly in phase; as expected, the contribution to temperature gradient variations by high-frequency internal waves is much less than for the displacement record. Vertical displacements and temperature gradient variations would be precisely in phase or in antiphase, as in the model, if upward and downward energy fluxes were equi-partitioned from moment to moment and if there were no phase randomization, such as is caused by nonlinear interactions (Mueller and Olbers, 1975).

Comparison of the normalized microstructure record and internal wave vertical shear inferred from temperature gradient variations (Fig. 14) suggests the first

and third lenses occurred near times of maximum shear. Interpretation of the third lens (Fig. 10) as a shear instability has been suggested in the earlier discussion; the situation is ambiguous with respect to the first lens (Fig. 6). The second microstructure lens (Fig. 9) occurs near a time of minimum internal wave shear and, as previously discussed, under conditions consistent with double-diffusive convection. Figs. 9 and 11 hint at a modulation of the double-diffusive convection by internal wave shear with maximum measured activity occurring near the time of minimum shear. No corresponding inverse effect of internal wave shear on the overall non-double-diffusive microstructure activity is found in this short record.

7. Discussion

A remarkable variety of thermal structures are observed in close juxtaposition in this short 20 h record at 550 m depth 500 km offshore. As has been seen, the regions of most intense mixing are closely associated

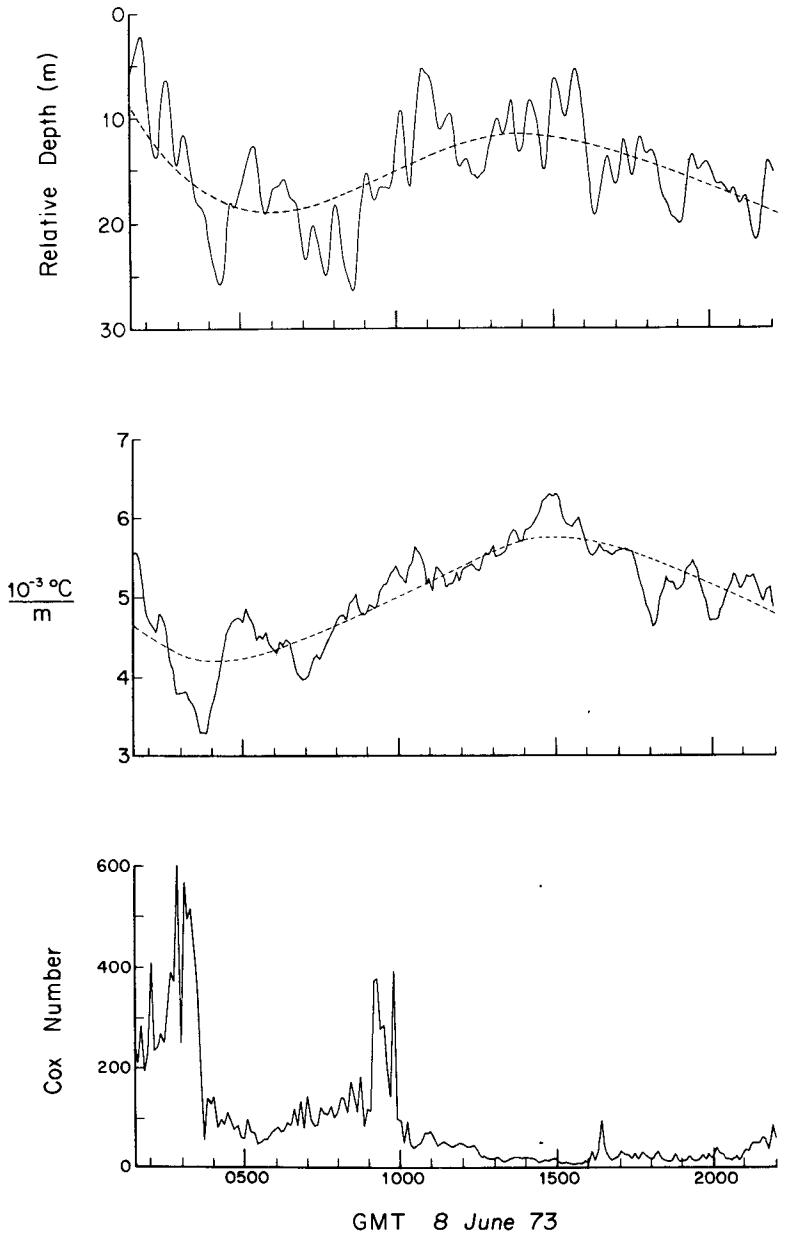

FIG. 14. Internal wave quantities and microstructure activity. (Top) Vertical displacements as indicated by the depth-time history of the 5.490°C isotherm. (Middle) Vertical strain as indicated by temperature gradients based on differences between top and bottom quartz thermometers, averaged over each profile. Smoothed curves have been added. (Bottom) Cox numbers as in Fig. 13.

with intrusive features; details of the observations hint that both shear instabilities and double-diffusive convection may be important in their dissipation.

The representativeness of the data discussed is uncertain. However, fragments of features similar in appearance to Fig. 6 (top) have also been found at 350 m (unpublished data) and at 800 m (Cairns, 1975) in other work with the capsule in the area. STD malfunctions prevented planned close-spaced casts to obtain direct information on the horizontal scales of the observed structures. STD casts were made, however, at the time of this experiment by Gregg on another ship a few kilometers distant from the capsule. At depths comparable to that of the capsule, these casts show a number of small intrusions of a few meters vertical extent on the otherwise smooth exponential-like profile.

Intrusions such as those found in the present data are short-lived with decay times of a few days at most (Table 1); therefore, the water masses forming the intrusions must be of local origin. Intrusive filaments extending from nearby, larger scale "parent" water masses, as seems to be the case in Fig. 9, are one source of such intrusions. Existing survey data are too widely spaced to be of help in identifying sources of such water masses, however. For example, at this depth, contours prepared using CCOFI STD stations (Gregg, 1975) yield only smooth features not readily associated with the present data.

Another possible source of intrusions, one not specifically identified in this record, is formation of an intrusion as the purely local result of gravitational collapse of a region mixed by gross internal wave breaking (cf Garrett and Munk, 1972b). The relative proportion of intrusions of the filament type, marking lateral water boundaries, and of the hypothesized collapse type, respectively, remain to be determined, as do the implications for oceanic mixing for a given mix of these processes.

Additional, longer term ($\sim$1 month) measurements are planned with the present system augmented to include conductivity and velocity sensors Such data, in combination with surveys to establish the larger context in which the float measurements are made, will allow more quantitative interpretations.

Acknowledgments. I am pleased to acknowledge the advice and guidance of Profs. Walter Munk and Charles Cox throughout this research. My thanks to Jim Cairns for help with aspects of the instrumentation and to Don Betts for valuable help with knotty, data display problems. I owe special thanks to Alan Chambliss who helped vitally with the capsule electronics in the initial, critical stages. This research was funded by the Advanced Research Projects Agency of the Department of Defense under contracts with the Scripps Institution of Oceanography.

REFERENCES

Cairns, J. L., 1975: Internal wave measurements from a midwater float. *J. Geophys. Res.*, **80**, 299–306.

Caldwell, D. R., F. E. Snodgrass and M. H. Wimbush, 1969: Sensors in the deep sea. *Physics Today*, **22**, 34–42.

Cox, C. S., P. W. Hacker, B. P. Johnson and R. T. Osborn, 1969: Fine scale of temperature gradient. *Trans. Marine Tech. Soc.*, **3**, 95–104.

Garrett, C. J. R., and W. H. Munk, 1972a: Space time scales of internal waves. *Geophys. Fluid Dyn.*, **3**, 225–264.

——, and ——, 1972b: Oceanic mixing by breaking internal waves. *Deep-Sea Res.*, **19**, 823–832.

——, and ——, 1975: Space-time scales of internal waves: A progress report. *J. Geophys. Res.*, **80**, 291–297.

Gregg, M. C., 1975: Microstructure and intrusions in the California current. *J. Phys. Oceanogr.*, **5**, 253–278.

——, and C. S. Cox, 1972: The vertical microstructure of temperature and salinity. *Deep-Sea Res.*, **19**, 355–376.

——, —— and P. W. Hacker, 1973: Vertical microstructure measurements in the Central North Pacific. *J. Phys. Oceanogr.*, **3**, 458–469.

Irish, J. D., and F. E. Snodgrass, 1972: Quartz crystals as multipurpose oceanographic sensors—I. Pressure. *Deep-Sea Res.*, **19**, 165–169.

Linden, P. F., 1973: On the structure of salt fingers. *Deep-Sea Res.*, **20**, 325–340.

Mueller, P., and D. J. Olbers, 1975: On the dynamics of internal waves. *J. Geophys. Res.*, **80**, 3848–3860.

Olson, J. R., 1972: Two-component electromagnetic flowmeter. *J. Marine Tech. Soc.*, **6**, 19–24.

Osborn, R. T., and C. S. Cox, 1972: Oceanic finestructure. *Geophys. Fluid Dyn.*, **3**, 321–345.

Pingree, R. D., 1972: Mixing in the deep stratified ocean. *Deep-Sea Res.*, **19**, 549–561.

Snodgrass, F. E., 1968: Deep sea instrument capsule. *Science*, **162**, 78–87.

Turner, J. S., 1973: *Buoyancy Effects in Fluids*. Cambridge University Press.

Woods, J. D., and R. L. Wiley, 1972: Billow turbulence and ocean microstructure. *Deep-Sea Res.*, **19**, 87–121.

Williams, G. O., 1975: Microstructure and internal wave measurements from a midwater float. Ph.D. dissertation, Scripps Institution of Oceanography, University of California, La Jolla.

——, 1976: Internal waves and horizontal coherence of finestructure (in preparation).